Causes of the Uncertainty in Projections of Tropical Terrestrial Rainfall Change: East Africa

DAVID P. ROWELL AND ROBIN CHADWICK

Met Office Hadley Centre, Exeter, United Kingdom

(Manuscript received 11 December 2017, in final form 5 April 2018)

ABSTRACT

Understanding the causes of regional climate projection uncertainty is a critical component toward establishing reliability of these projections. Here, four complementary experimental and decomposition techniques are synthesized to begin to understand which mechanisms differ most between models. These tools include a variety of multimodel ensembles, a decomposition of rainfall into tropics-wide or region-specific processes, and a separation of within-domain versus remote contributions to regional model projection uncertainty. Three East African regions are identified and characterized by spatially coherent intermodel projection behavior, which interestingly differs from previously identified regions of coherent interannual behavior. For the ''Short Rains'' regions, uncertainty in projected seasonal mean rainfall change is primarily due to uncertainties in the regional response to both the uniform and pattern components of SST warming (but not uncertainties in the global mean warming itself) and a small direct CO_2 impact. These primarily derive from uncertain regional dynamics over both African and remote regions, rather than globally coherent (thermo)dynamics. For the ''Long Rains'' region, results are similar, except that uncertain atmospheric responses to a fixed SST pattern change are a little less important, and some key regional uncertainties are primarily located beyond Africa. The latter reflects the behavior of two outlying models that experience exceptional warming in the southern subtropical oceans, from which large lower-tropospheric moisture anomalies are advected by the mean flow to contribute to exceptional increases in the Long Rains totals. Further research could lead to a useful assessment of the reliability of these exceptional projections.

1. Introduction

Extremes of tropical rainfall, whether they are droughts or floods, can be catastrophic in developing countries. Poor infrastructure and a dependence on local agriculture leave vulnerable populations exposed. Over the coming decades, climate models predict that ongoing anthropogenic emissions will lead to sizable changes in the frequency, intensity, and spatiotemporal distribution of such events (Collins et al. 2013). However, while these models provide confidence that many tropical regions will experience large changes in rainfall (Chadwick et al. 2016a), they disagree on the pattern of change. Thus, for any specific location, predictions of the amplitude of rainfall change—and sometimes its sign—are highly uncertain. This adds to the challenge of making robust development decisions, such as building new infrastructure resilient to climate change over the coming decades. This study, therefore, aims to improve our understanding of the causes of the uncertainties in projected regional rainfall change and so contribute to the development of performance metrics that can be employed to subselect models in a way that is tailored to the mechanisms most relevant to their projections of future change.

Understanding of the physical mechanisms that determine the response of regional tropical rainfall to rising carbon emissions has advanced considerably over recent years. The impact of enhanced atmospheric CO_2 concentrations is usually expedited via the slow warming of the global oceans, although in some regions, direct radiative effects on the troposphere and land surface

Denotes content that is immediately available upon publication as open access.

Corresponding author: David P. Rowell, dave.rowell@metoffice.gov.uk

DOI: 10.1175/JCLI-D-17-0830.1

also lead to notable changes in local climate and rainfall (e.g., Cao et al. 2012; Bony et al. 2013; Merlis 2015; He and Soden 2016). With regard to influences on tropical terrestrial rainfall via oceanic warming, a number of mechanisms have been proposed that operate (to a greater or lesser extent) throughout the tropics: ''wet get wetter, dry get drier'' (also referred to as the M′ mechanism; e.g., Held and Soden 2006; Chou et al. 2009; Chou and Neelin 2004); ''warm get wetter'' (e.g., Xie et al. 2010; Ma and Xie 2013; Chadwick et al. 2014); ''upped ante'' or enhanced moist stability over land (Chou and Neelin 2004; Chou et al. 2009; Giannini 2010); thermodynamic moisture increases advected over land (Chadwick et al. 2016b), contrasting with reductions in near-surface relative humidity (RH) over land (e.g., Rowell and Jones 2006; Fasullo 2010; Byrne and O'Gorman 2016; Chadwick et al. 2016b); tropics-wide weakening of the mean circulation (e.g., Held and Soden 2006; Ma et al. 2012); and interhemispheric asymmetry in the surface and atmospheric energy budgets (e.g., Kang and Held 2012). In addition, regionally specific mechanisms are also critical: these include teleconnections from climate change in either nearby or remote regions [including anomalous patterns of sea surface temperature (SST)], changes to the teleconnections themselves, and the impact of—and changes to—local feedback mechanisms, such as interactions with the land surface or clouds (e.g., Berg et al. 2016; Chou and Neelin 2004; Voigt et al. 2014).

Nevertheless, it is unclear which of these mechanisms is most responsible for uncertainties in regional tropical rainfall projections. Most studies to date have taken a generic tropics-wide view, and yet, despite the advances encapsulated above, few have focused on the drivers of uncertainty in specific tropical regions. Here, we focus on East Africa, where the rapidly growing and ill-equipped population has suffered considerably in the face of recent droughts and floods (e.g., Hillbruner and Moloney 2012; Mason et al. 2012; Nicholson 2016, 2017) and urgently needs to become more resilient to future change. That said, it is also intended that the multifaceted approach presented here might be applicable to other tropical terrestrial regions.

The scope of this study is, however, necessarily limited. In particular, we focus on the seasonal mean rainfall response to well-mixed greenhouse gases (primarily CO_2) rather than also considering changing aerosol emissions. This comes partly as a consequence of analyzing late-twenty-first-century data to maximize signal-to-noise ratios, at which time CO_2 dominates the radiative response. It is also a choice that derives from recent research showing that the role of aerosols on East African climate is unknown, at least in the context of recent change (Rowell et al. 2015). In terms of the language of this study, an important distinction is that we shall use ''uncertainty'' to mean only the spread across CMIP5 projections, whereas in practice, we recognize that other uncertainties may also be critical, in particular the effects of parameterized convection, coupling with East Africa's Great Lakes, and the local response to growing urban land use. All these are being addressed by related studies, outlined by Marsham et al. (2015).

The aim of this study is, therefore, to determine the ''top level'' causes of uncertainty among models in their projections of seasonal mean rainfall change in each of East Africa's two main wet seasons: the ''Long Rains'' of March to May (MAM) and the ''Short Rains'' of October to December (OND). We utilize four complementary experimental and decomposition techniques, each with its own advantages and focus. The questions addressed work through a process chain from the initial CO_2 impact of altered radiative forcing to global-scale responses and then regional-scale responses. After describing the data and selecting appropriate regions (section 2), we ask four questions: Are the projection uncertainties over East African due more to the uncertainty in direct or indirect (via ocean warming) responses to rising carbon emissions (section 3); due more to uncertainty in the uniform or pattern component of SST change (section 4); due more to uncertainty in globally coherent or regionally specific mechanisms (section 5); and last, due more to uncertainty in local or remote mechanisms (section 6)? The answers to these suggest immediate further analysis of the Long Rains season (section 7), which is followed by our conclusions (section 8).

2. Model data and regional definitions

a. Climate model data

Four suites of climate model experiments are utilized in this study, sourced from phase 5 of the Coupled Model Intercomparison Project (CMIP5; Taylor et al. 2012) and the Coordinated Regional Climate Downscaling Experiment (CORDEX; Giorgi et al. 2009; Jones et al. 2011). Details are as follows.

Coupled atmosphere–ocean simulations forced by representative concentration pathways (RCPs) aim to project future climate change with as much realism as possible. Our focus is on simulations forced by the high-emissions RCP8.5 scenario, since this has good data availability and large signal-to-noise ratios. Forty models archived monthly mean precipitation data to the CMIP5 database (Table 1), along with most other variables required in this study. For each model, anomalies

TABLE 1. Availability of CMIP5 experiments or data and the branch year of abrupt4xCO_2. For the latter, "same" means that labeling of abrupt4xCO_2 years matches that of the corresponding piControl years; otherwise, the numbers are the piControl year from which the first year of abrupt4xCO_2 branches. Expansions of model acronyms are available at http://www.ametsoc.org/PubsAcronymList.

Model name/version	RCP8.5 and historical	Abrupt4xCO2 and piControl	(Thermo)dynamic decomposition	Atmos. only
ACCESS1.0	✓	✓ same	✓	
ACCESS1.3	✓	✓ same	✓	
BCC_CSM1.1	✓	✓ same	✓	✓
BCC_CSM1.1(m)	✓	✓ same	✓	
BNU-ESM	✓	✓ same	✓	
CanESM2	✓	✓ 2321	✓	✓
CCSM4	✓	✓ 251	✓	✓
CESM1(BGC)	✓		✓	
CESM1(CAM5)	✓		✓	
CMCC-CESM	✓			
CMCC-CM	✓			
CMCC-CMS	✓			
CNRM-CM5	✓	✓ same	✓	✓
CNRM-CM5.2		✓ 1960		
CSIRO Mk3.6.0	✓	✓ 104	✓	
EC-EARTH	✓			
FGOALS-g2	✓	✓ same	✓	
FIO-ESM	✓		✓	
GFDL CM3	✓	✓ same	✓	
GFDL-ESM2G	✓	✓ same	✓	
GFDL-ESM2M	✓	✓ same	✓	
GISS-E2-H	✓	✓ 2660	✓	
GISS-E2-H-CC	✓		✓	
GISS-E2-R	✓	✓ 4200	✓	
GISS-E2-R-CC	✓		✓	
HadGEM2-AO	✓		✓	✓
HadGEM2-CC	✓		✓	
HadGEM2-ES	✓	✓ same	✓	
INM-CM4.0	✓	✓ same	✓	
IPSL-CM5A-LR	✓	✓ same	✓	✓
IPSL-CM5A-MR	✓	✓ same	✓	
IPSL-CM5B-LR	✓	✓ same	✓	✓
MIROC-ESM	✓	✓ 1880	✓	
MIROC-ESM-CHEM	✓		✓	
MIROC5	✓	✓ same	✓	✓
MPI-ESM-LR	✓	✓ 1880		✓
MPI-ESM-MR	✓	✓ same		✓
MPI-ESM-P		✓ same		
MRI-CGCM3	✓	✓ 1891	✓	✓
MRI-ESM1	✓		✓	
NorESM1-M	✓	✓ 700	✓	
NorESM1-ME	✓		✓	

are computed from a "historical" simulation that imitates recent climate variability by using realistic anthropogenic and natural forcings. Data are averaged over 2070–99 and 1950–99, respectively, to balance the competing needs of reduced sampling noise and limited trends.

The "abrupt4xCO_2" experiment also employs the fully coupled ocean–atmosphere version of each climate model but is highly idealized. Its forcing consists of an initial instantaneous quadrupling of the atmospheric CO_2 concentration, which is then held constant throughout the run, a minimum of 140 years. Data are available for 28 climate models from the CMIP5 archive (as well as one further model that was not processed here due to substantial metadata issues); see Table 1. The abrupt4xCO_2 experiment was initialized from and is compared with the preindustrial control (piControl) experiment, in which the atmospheric CO_2 concentration is fixed at a preindustrial level. All other external forcings in both experiments are fixed at preindustrial conditions. An important analysis parameter is the time at which the abrupt4xCO_2 run branches from the piControl because this enables computation of anomalies that are not contaminated by an initial excess of random

TABLE 2. CORDEX GCM–RCM model combinations available for both the RCP8.5 and historical simulations.

GCM \ RCM	SMHI RCA4	MPI REMO2009	DMI HIRHAM5	CLMcom CCLM4.8.17	KNMI RACMO22T
CanESM2	✓				
MIROC5	✓				
CNRM-CM5	✓			✓	
CSIRO Mk3.6.0	✓				
EC-EARTH	✓	✓	✓	✓	✓
MPI-ESM-LR	✓	✓		✓	
NorESM1-M	✓		✓		
HadGEM2-ES	✓			✓	✓
GFDL-ESM2M	✓				
IPSL-CM5A-LR		✓			
IPSL-CM5A-MR	✓				

internal variability. However, this parameter is not always present in the models' metadata and is ambiguous or unreliable for some models, so a method to check or determine it from SST data is presented in appendix A.

A further suite of idealized experiments uses an atmosphere-only version of each climate model [atmospheric general circulation model (AGCM)]. These are variants of the standard Atmospheric Model Intercomparison Project (amip) experiment, which is forced by observed 1979 to 2008 SSTs and observed atmospheric constituents. Three such coordinated experiments are used here: "amip4K" differs from amip in that a globally uniform 4 K SST anomaly is added to the marine surface, and "amipFuture" differs by including a climatological SST pattern anomaly taken from the ensemble mean of the CMIP3 1% yr^{-1} CO_2 increase experiments, centered on the time of CO_2 quadrupling and scaled such that the global mean SST anomaly is 4 K, with the same SST pattern applied to all models. Last, "amip4xCO_2" differs in that its atmospheric CO_2 concentration is quadrupled throughout the experiment. Data from 11 models are available for all these experiments, as listed in Table 1. The computed anomalies in this study are "amip4K minus amip," "amipFuture minus amip4K" (to examine the impact of the SST pattern change alone), and "amip4xCO_2 minus amip," with data averaged over all years of each experiment.

Last, we also utilize data from the CORDEX-Africa regional climate model (RCM) projections, forced by the RCP8.5 scenario. A number of different RCMs have been run on a common African domain (e.g., Nikulin et al. 2012) and resolution, forced at their lateral and marine boundaries by data from a range of global climate models (GCMs). The available GCM–RCM combinations are shown in Table 2. Anomalies are computed from analogous historical simulations, and data are averaged over 2069–98 and 1952–2001.

For all experiments (past and future), only the first member of initial condition ensembles is analyzed for consistency among models. Also, to facilitate a multimodel analysis (as well as enhance signal-to-noise ratios in the CORDEX analysis), all data are interpolated to a common grid: that of HadGEM2-ES, which is 1.25° latitude × 1.875° longitude. Last, all analyses were repeated for a multimodel subensemble restricted to one model per institute to assess the impact of using a more independent, but smaller and incomplete, sample of models (cf. Knutti et al. 2013; Sanderson et al. 2015). All conclusions were unaffected.

b. *Analysis regions, analysis seasons, and model spread*

Spatial averages are useful for reducing the impact of small-scale noise and focusing attention on the region of interest. However, results can be sensitive to the precise definition of these regions, so it is worth giving this careful consideration. As stated in the introduction, our objective is to better understand the causes of uncertainty in rainfall projections over East Africa. Thus, we want to delineate regions and seasons such that the differences between any pair of models' projections are broadly consistent across the region and between months, so that averages encompass similar intermodel behavior. An important consequence is that the drivers and mechanisms of projection uncertainty will likely be coherent across the region and thereby easier to isolate. Furthermore, if these dominant processes differ from those predominantly responsible for natural interannual variability, then we should not be surprised that appropriate regions for these two applications may differ rather than being interchangeable.

Statistically, we require the intermodel correlations of rainfall anomalies between gridpoint pairs to be high

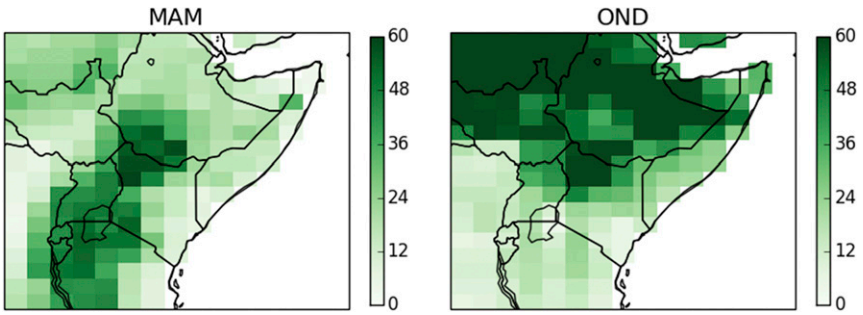

FIG. 1. Spatial coherence of intermodel variations of projected precipitation anomalies for MAM and OND using 40 CMIP5 models. Datum at each grid point is the number of other points for which the intermodel correlation with the base point exceeds 0.707 (>50% common variance).

within each of the regions we define. First, we compute these correlations (r) between all gridpoint pairs across East Africa, using RCP8.5-minus-historical rainfall data. To be clear, these correlations quantify the relationship between 40-element data arrays (since we have 40 models), then are repeated for all pairs of grid points. Next, Fig. 1 shows at each grid point and each wet season the number of other grid points correlated to this base point at $r > 0.707$; this is the number of grid points with more than 50% common variance with the base point, in terms of the relative behavior of models' projected rainfall anomalies. Pale colors show where relative intermodel behavior is similar to only a few other grid points, suggesting spatial independence of projection behavior from the majority of the domain: that is, different primary mechanisms governing the relative ranking of models across the CMIP5 ensemble (or alternatively, a high impact of sampling variability). Conversely, dark colors suggest spatial coherence across a larger portion of the domain and common primary mechanisms driving intermodel differences in rainfall response over a sizable region. It is, therefore, these latter areas that can be used as a guide toward defining appropriate spatial averaging regions.

Five criteria are used to define these averaging regions: 1) preference for large spatial extent; 2) inclusion of Lake Victoria, where the high population density is predicted to continue rising rapidly (Seto et al. 2012) and because our study contributes to a project aiming to assist stakeholders in the Lake Victoria basin make climate-resilient development decisions (Marsham et al. 2015; https://hycristal.wordpress.com/); 3) all points within the region must have at least 50% common cross-ensemble variance with at least 50% of the other points; 4) all grid points experience their wettest month during one of the transition seasons using Nicholson's (2014) analysis, which is used to exclude large areas of North Africa during the Short Rains; and 5) the region is contiguous, such that all grid boxes are adjacent to another on at least two edges. The resulting averaging regions are shown in the upper panels of Fig. 2. They consist of a large region for the Long Rains (EA-LR) (MAM), a large region for the Short Rains (EA-SR) (OND), and a further small region for the Short Rains to investigate uncertainties around Lake Victoria (LV-SR). By design, spatial coherency of intermodel behavior is good within each region, with average intermodel correlations between gridpoint pairs being 0.63, 0.78, and 0.75, respectively. We also note that these regions indeed differ substantially from those used to study interannual variability [e.g., the Greater Horn of Africa defined by Rowell (2013) using a similar methodology on gridded observed rainfall data], suggesting that drivers of projection uncertainty may be very different from those that dominate the regional response to natural variations internal to the climate system.

It is also necessary to assess the intraseasonal coherency of the relative behavior of models across the CMIP5 ensemble. Month-to-month correlations within the wet season relevant to each region show at least 50% common variance for the two large regions ($0.70 < r < 0.88$) but are a little less for the smaller Lake Victoria region ($r = 0.69, 0.64$), presumably due to larger sampling effects. We therefore judge this intraseasonal coherency to be sufficient to average data over the 3 months of each wet season, rather than subdividing them and increasing sampling noise. Note also that each region is only used with data from the wet season to which it corresponds, although we will sometimes omit this information for brevity.

The black dots in the lower panels of Fig. 2 illustrate the spread of the projected seasonal rainfall anomalies for each region in the late twenty-first century under the RCP8.5 emissions scenario. The majority of models predict an increase in seasonal mean rainfall for all regions and both seasons, as found by many other studies

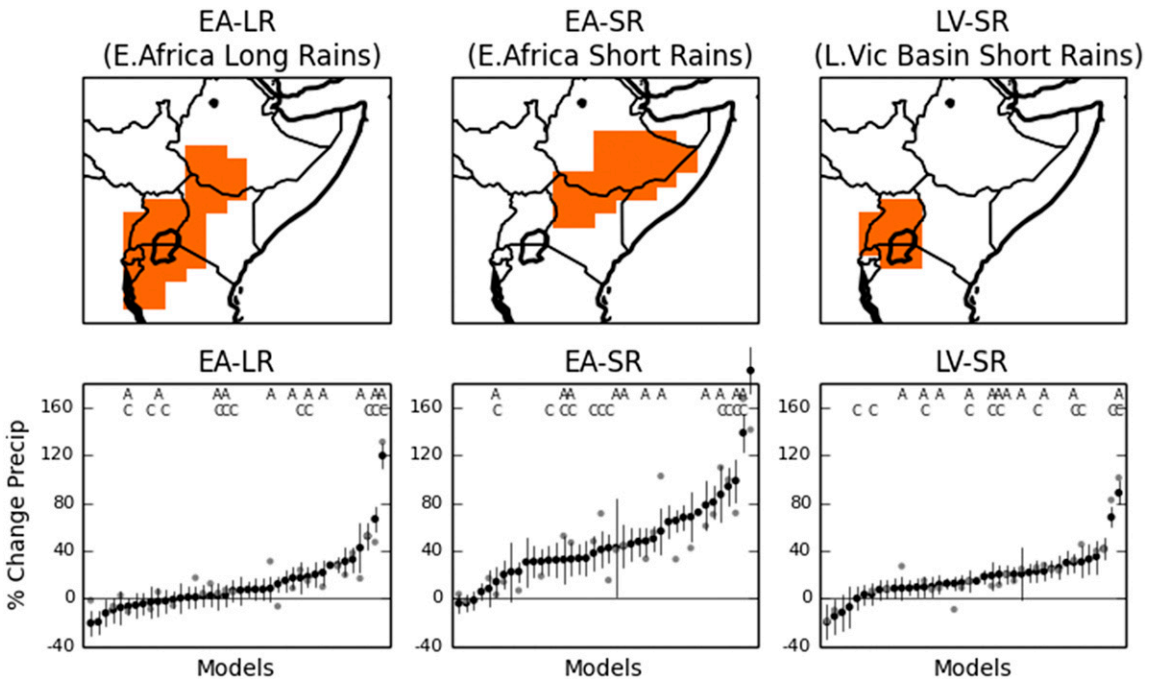

FIG. 2. (top) The averaging regions used in this study. (bottom) Black dots show the projected percentage change in precipitation for RCP8.5-minus-historical, with models (each dot) in rank order. Vertical lines show ±2 SD of natural variability for 30- minus 50-yr anomalies, computed from piControl. Gray dots show rainfall change for abrupt4xCO_2 (years 111–140) minus piControl (average of all years), scaled to the same global annual mean temperature anomaly as each model's RCP8.5 anomaly. Letters A and C indicate the availability of AGCM and CORDEX experiments for each model.

(e.g., Shongwe et al. 2011; Otieno and Anyah 2013; Rowell et al. 2015). This tendency is strongest for the EA-SR region. Furthermore, the spread across the CMIP5 models is substantial, with the majority of projection anomalies spanning a range of 90%, 100%, and 60% of the recent climatology for the three regions, respectively. This is problematic for adaptation decisions, increasing risks and/or costs for already poor nations. Beyond this ''range of the majority'' also lies one or two outlier projections. A critical question for climate science is whether or not these outliers must be treated as equally plausible alongside other models.

A final foundational question to ask of the East African rainfall data is whether the relative behavior of models is consistent between the regions. Intermodel (cross ensemble) correlations between regions are 0.20, 0.46, and 0.63 (EA-LR–EA-SR, EA-SR–LV-SR, and LV-SR–EA-LR, respectively), or 0.29, 0.57, and 0.18 when the two largest outliers are removed from each region. These fairly low values imply large interregional and interseasonal differences in the dominant processes that drive projection uncertainty, more so than the interregional commonality, thus requiring that these regions and seasons should be examined separately.

3. Direct versus indirect CO_2 mechanisms

The first stage of the mechanistic chain is whether uncertainties in projected regional change are driven more by uncertainties in the direct radiative effects of enhanced CO_2 concentrations or more by uncertainties in indirect effects, where the latter refers to uncertainties in the warming of the oceans and in the atmospheric response to that warming. A powerful tool to address this question is CMIP5's coordinated abrupt4xCO_2 experiment, described in section 2a and available for 28 coupled climate models. This allows us to disentangle these two very different mechanistic groups by analyzing the response rate of a regional climate metric to the instantaneous quadrupling of atmospheric CO_2 concentration. Time scales are clearly distinct, with direct radiative responses typically developing within a few weeks (Dong et al. 2009; Cao et al. 2012) and indirect effects (via SST responses) developing steadily over many decades due to the slow heat uptake of the oceans.

First, we check that the quasi-equilibrium response of these experiments—when both mechanistic groups are fully established—is representative of their response in the more realistic RCP8.5 projections. The

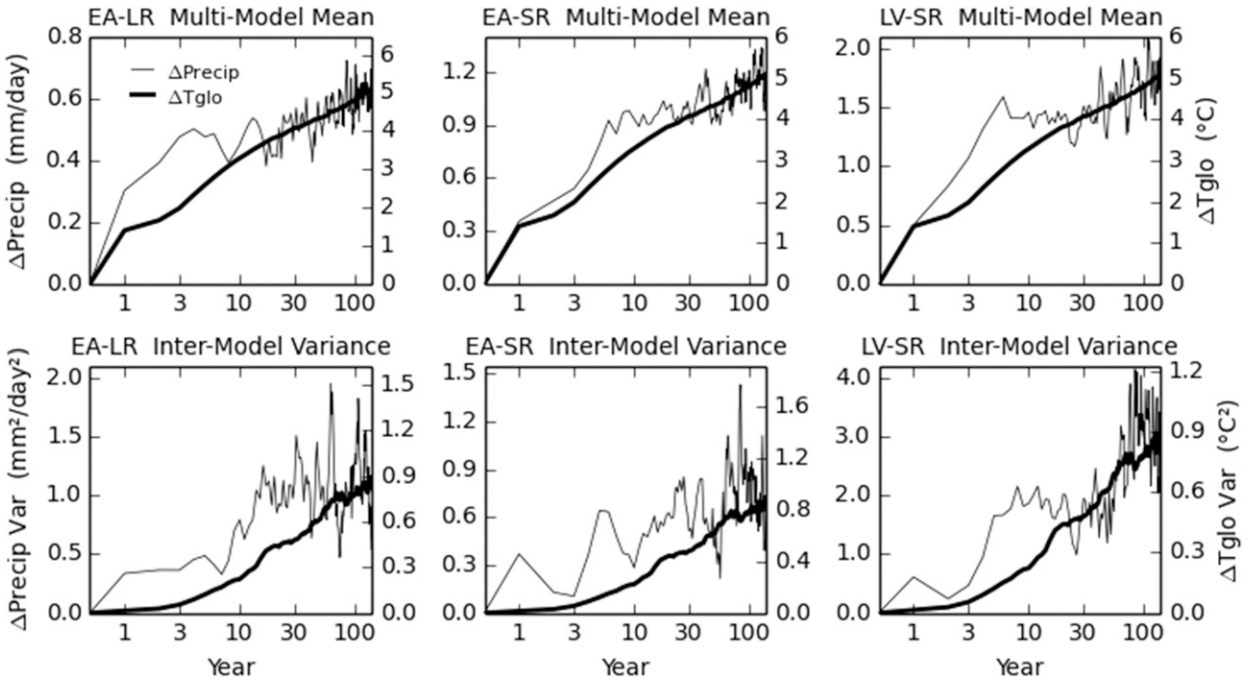

FIG. 3. Evolution of the abrupt4xCO_2 minus piControl area-average rainfall anomaly for three East African regions (thin line) and global annual mean surface air temperature (thick line). (top) Multimodel ensemble means and (bottom) intermodel variance are computed for each year. Data are smoothed with a 5-yr running mean, and the two *y* axes are scaled to match averages over the last 30 years.

abrupt4xCO_2 anomalies, scaled by the ratio of the RCP8.5-to-abrupt4xCO_2 global mean temperature change, are shown by the gray dots in the lower panels of Fig. 2. These are well correlated with the RCP anomalies (r = 0.92, 0.87, and 0.95 for EA-LR, EA-SR, and LV-SR, respectively), with a majority of individual model differences falling within the internal variability of the coupled climate system. This smaller sample of 28 models is also distributed evenly across the range of RCP anomalies, including the outliers. Thus, the equilibrium state of the abrupt4xCO_2 experiments is a suitable proxy for the RCP projections, as well as evidence of the dominant forcing role of the CO_2 burden in the late twenty-first century.

The evolution of East Africa's ensemble mean rainfall response is shown in the upper row of Fig. 3, using a logarithmic *x* axis and 5-yr smoothing of the data (with points at the array edges given extra weight). In all three regions, rainfall anomalies (thin line) evolve steadily, at a similar time scale to the global mean warming (thick line), rather than at the rapid time scale of direct radiative responses. Nevertheless, a more precise interpretation of Fig. 3 is that it also suggests a slightly faster evolution of East African rainfall anomalies than that of global mean warming. This difference slightly exceeds the bounds of natural variability, judged by the amplitude of variations along the remainder of the Fig. 3 curves. Given this result is also consistent among the three regions, we speculate that it may be physically based rather than a random sampling effect. One hypothesis could be that anomalous SST patterns play a secondary role, since these develop more rapidly than the mean warming (Chadwick et al. 2014; Long et al. 2014). This is addressed in section 4.

Nevertheless, the key question addressed by this study is not which mechanisms drive the multimodel ensemble mean response, but rather which mechanisms differ most between models, such that they lead to uncertain East African rainfall changes across the CMIP5 ensemble. Thus, the lower panels of Fig. 3 show the temporal evolution of the component of intermodel variance due to modeling formulation. This is computed from the cross-ensemble variance of each year of the smoothed abrupt4xCO_2-minus-piControl anomalies, from which twice the variance found in the smoothed piControl data is subtracted [to remove the contribution of natural variations in the abrupt4xCO_2 and piControl; see Rowell (2012) for further explanation]. Figure 3 suggests that to first order, the time scale of the primary drivers of intermodel uncertainty also follows the time scale of the evolving uncertainty in global mean warming, more than that of the rapidly evolving uncertainty in

direct radiative responses. Initial direct responses contribute 30 ± 5%, 28 ± 15%, and 15 ± 5% of the total intermodel variance for EA-LR, EA-SR, and LV-SR, respectively, measured here by the ratio of variance averaged over years 1–3 divided by that of years 101–140 and dropping each model in turn to estimate a maximum error bar. Note that if data are unsmoothed (not shown), then identical conclusions are drawn, with no dominant variances apparent in the first year alone. There is also a notable secondary influence of uncertain mechanisms that respond to enhanced CO_2 concentrations over an initial multidecadal time scale. To quantify this, we first compute that at years 11–30, the uncertainty in the response to global warming contributes only 60% ± 10%, 57% ± 7%, and 88% ± 10%, respectively, to the total uncertainty (computed as the ratio of the variance of global mean warming averaged over years 11–30 divided by that in years 101–140, then scaled by the same calculation for regional rainfall data). The remainder (40% ± 10%, 43% ± 7%, and 12% ± 10%, respectively) is then that due to uncertainties in both the initial direct response to CO_2 and the subsequent multidecadal response.

Last, it is important to note that this first-order temporal relationship between the models' local rainfall anomalies and their global warming anomalies (and the consequential relationship between intermodel variances) does not imply that at a specific time point (and scenario) there is a similar intermodel relationship between the relative amplitude of a model's global warming and its East African rainfall anomaly. Indeed, cross-ensemble correlations between global mean warming and East African rainfall change are 0.31 to 0.47, using abrupt4xCO_2 anomalies averaged over years 111–140. So, the modeling uncertainty in East African climate change at a specific time point is driven much more by uncertainty in the regional response to global warming than by uncertainty in the global warming itself. This is typical of other tropical regions (Rowell 2012; Kent et al. 2015).

4. Uniform SST warming versus SST pattern changes

Next, one might ask which aspects of the SST warming most strongly affect the uncertain regional response. Are uncertainties in East African rainfall change primarily related to the uniform component of SST warming, or to changes in SST patterns? And does this balance vary seasonally and regionally? CMIP5's coordinated idealized AGCM experiments, described in section 2a, were designed to answer these questions. They are available for 11 models, marked by "A" in Fig. 2, which show these models to be evenly spread through the distribution of projected East African rainfall anomalies, including high outliers, although less representative of the lowest quartile. Note, however, that the experimental design does not include the impact of intermodel variations in the SST base state or pattern change, since the amipFuture experiment uses a fixed SST pattern added to an observed SST climatology. Additionally, the influences of the AGCMs' lack of ocean–atmosphere coupling and plant physiological responses to CO_2 cannot be assessed, although He and Soden (2016) and Chadwick et al. (2017) show these may be secondary over East Africa. Nevertheless, Chadwick et al. (2014) show there to be reasonable similarity between the long-term ensemble mean coupled response over land and the sum of the amipFuture and amip4xCO_2 anomalies.

Figure 4 shows the AGCM experiments' ensemble mean rainfall response across Africa and the Indian Ocean, using data for each model averaged over all available years. Uniform SST warming tends to enhance rainfall over the ocean due to the enhanced heat and moisture flux into the lower troposphere, and it reduces rainfall over land due to warming aloft in response to the enhanced oceanic diabatic heating and reduced RH arising from increased land–sea temperature gradients (Held et al. 2005; Bayr and Dommenget 2013; Fasullo 2012, respectively). The SST pattern change includes some further warming of the Indian Ocean (not shown) so similarly enhances rainfall here, whereas an El Niño–like SST pattern induces a rainfall decline over and around the Maritime Continent. We caution, however, that this is only one plausible SST pattern response; different patterns would likely produce different responses. Also shown is the impact of enhanced CO_2 alone (with unaltered SSTs), which tends to enhance rainfall over land, due to both atmospheric and surface warming from increased downwelling longwave radiation, and reduce rainfall over the ocean, due to increased atmospheric stability and weakening of the tropical circulation in the absence of enhanced surface warming (Sugi and Yoshimura 2004; Merlis 2015, respectively).

The contributions of these mechanisms to intermodel uncertainty in rainfall response are shown in Fig. 5. Also printed are results for data first averaged over our East African regions, where the maps suggest uncertainties are driven by a mix of oceanic and continental influences; this mix itself is also model dependent. Although the East African ensemble mean response is small (Fig. 4), the responses of individual models vary considerably and significantly exceed natural variability for an average of 8 out of 11 models (computed using the Student's t test against the null hypothesis that forced

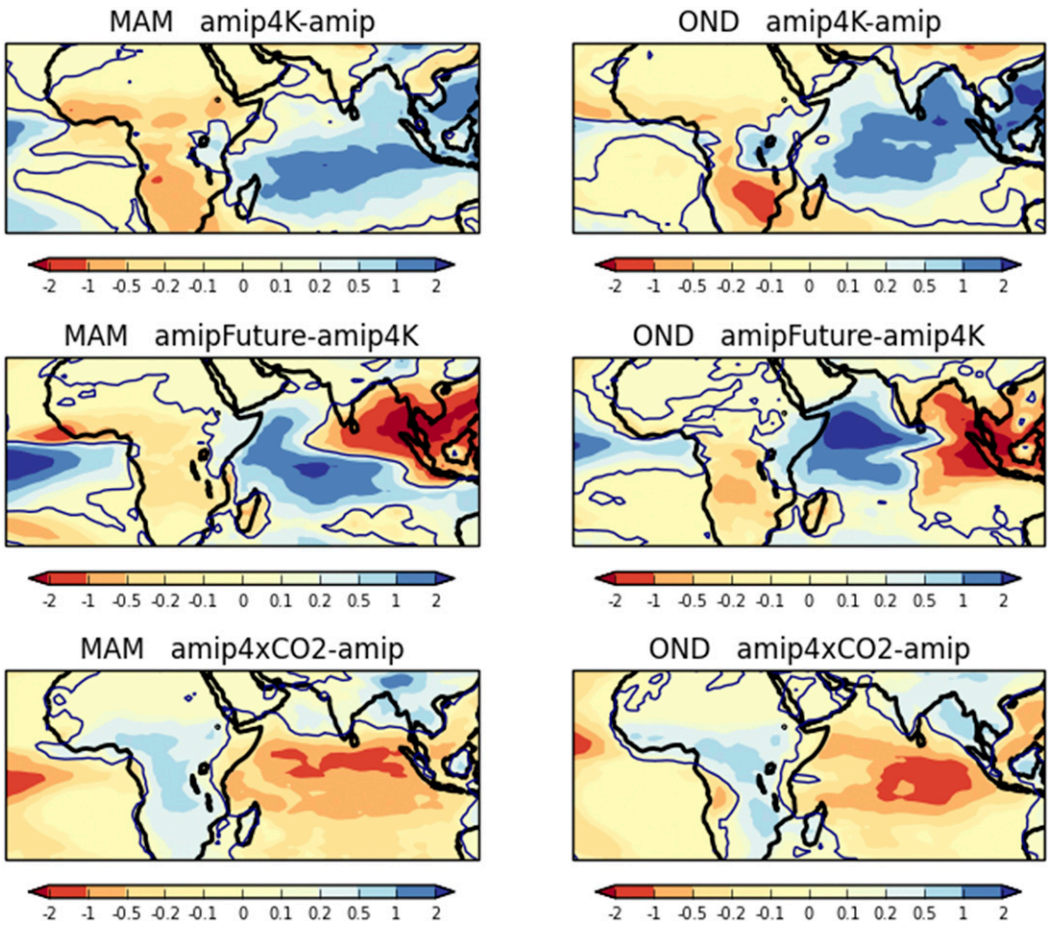

FIG. 4. Multimodel ensemble means of the seasonal mean precipitation response in idealized AGCM experiments.

responses derive from the same population as differences between same-model members of amip initial condition ensembles, using data from the four models that have at least five ensemble members). Note, too, that the following evaluation of interexperimental differences in uncertainty over East Africa is robust to removal of each of the three most outlying models.

During the Long Rains, uncertainties in regional rainfall change are primarily determined by uncertain responses to the uniform warming of the ocean, with a secondary role played by the SST pattern change (Fig. 5). Both components of this SST response depend on the uncertain modeling of ocean–atmosphere fluxes, boundary layer processes, atmospheric convection, and land–atmosphere exchanges. In contrast, uncertainty in the direct effects of rising CO_2 is much smaller, echoing the findings of the abrupt4xCO_2 coupled model experiment (section 3).

During the Short Rains, uncertainties in the models' responses to both the uniform and pattern components of SST warming contribute strongly to uncertainty in East African rainfall change. This larger role for anomalous SST patterns, compared to the Long Rains, is physically plausible, given the Short Rains' much larger interannual sensitivity to anomalous SSTs (e.g., Ogallo et al. 1988; Camberlin and Philippon 2002). However, further testing is required, for which the improved CMIP6 AGCM experimental design (Chadwick et al. 2017) will be useful. Regarding the direct effects of CO_2 (not via oceanic warming), this plays a secondary role as a driver of uncertainty (cf. section 3), although it may not be as small as during the Long Rains.

5. Thermodynamic versus dynamic mechanisms

We now evaluate the contributions of some overarching global and regional mechanisms to the uncertainty in projected East African rainfall change—in particular, the roles of two thermodynamic and two dynamic mechanisms. In this case, a diagnostic approach is applied to the CMIP5 RCP8.5 simulations, the model integrations often employed to project future climate

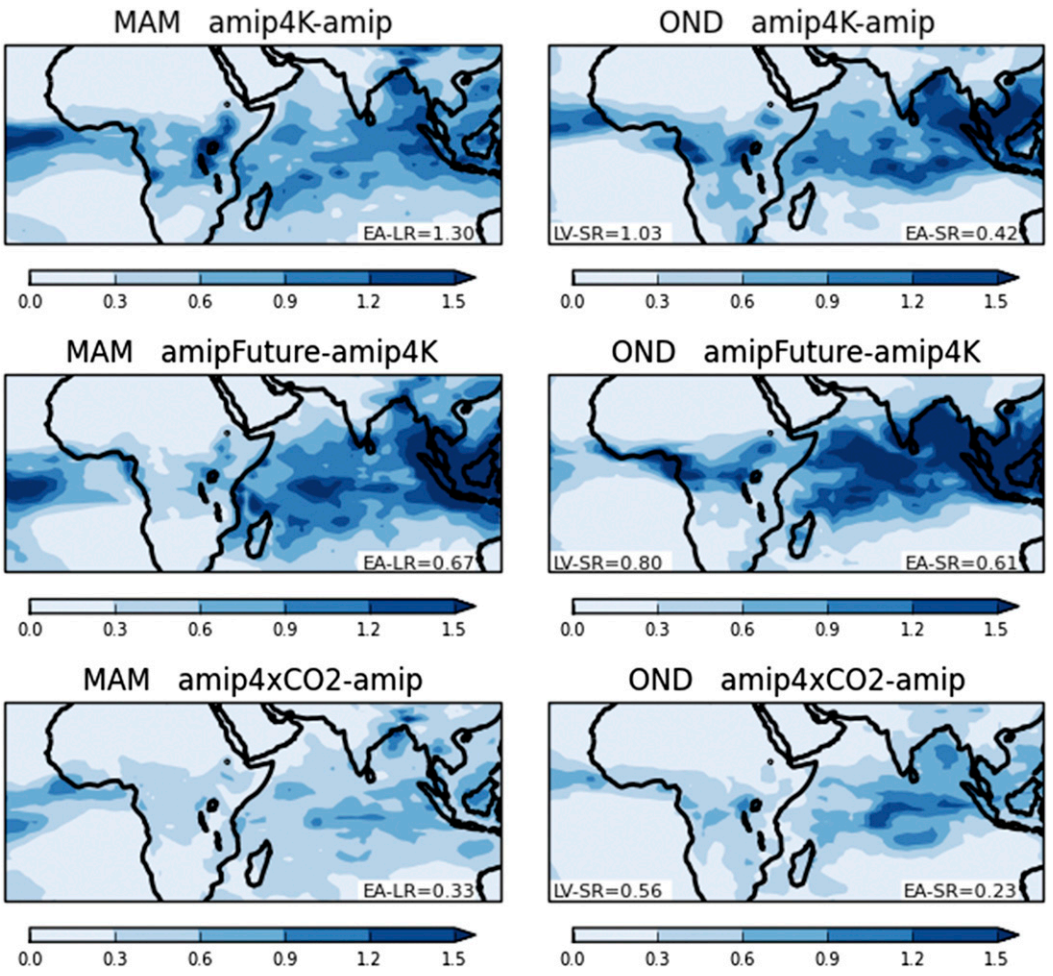

FIG. 5. Intermodel standard deviation of the seasonal mean precipitation response in idealized AGCM experiments. Text inserts are standard deviations for data first averaged over the three East African regions.

change using fully coupled systems. The necessary variables are available from 34 models (Table 1).

The decomposition framework is that of Chadwick et al. (2016b), an update of that originally developed by Chadwick et al. (2013). It is founded on the following assumptions:

(i) Precipitation can be equated to the multiple of boundary layer specific humidity (q) and mass flux (M) from the boundary layer to the free troposphere [Held and Soden (2006 and Kent et al. (2015) show this to be valid for climatological monthly mean data in the tropics].

(ii) The change in q (Δq) over land can be partitioned into a component due to increased maritime moisture advection onto land (where q_{land} is scaled by the zonal mean fractional change in q_{ocean} at the same latitude, with no circulation change) and a residual associated with changes in circulation, evaporation, and vertical mixing [Chadwick et al. (2016b) show this to be valid in the tropics].

(iii) Circulation change in the tropics can be partitioned into a component associated with the mean weakening of the tropical circulation and a residual associated with spatial shifts in convection [Chadwick et al. (2013) and Kent et al. (2015) show this to be a reasonable description of CMIP5 behavior].

Each model's monthly mean precipitation anomalies (ΔP) are then decomposed as

$$\Delta P = \Delta P_{\text{qadv}} + \Delta P_{\text{res}} + \Delta P_{\text{weak}} + \Delta P_{\text{shift}} + \Delta P_{\text{cross}},$$

which are its components due to the change in q_{land} arising from increased moisture advection from the oceans (ΔP_{qadv}), residual changes in q_{land} (ΔP_{qres}), the tropics-wide circulation weakening (ΔP_{weak}), spatial shifts in convection (ΔP_{shift}), and a nonlinear cross term

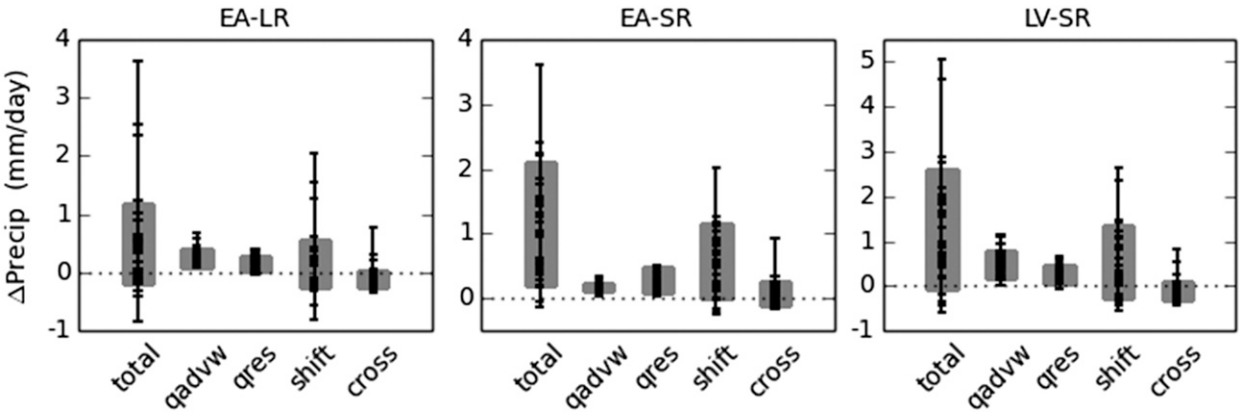

FIG. 6. Decomposition of RCP8.5-minus-historical precipitation change into dynamic and thermodynamic components, averaging data over the three East African regions. Tick marks on each vertical line show results for individual CMIP5 models, and gray bars mark approximately the central 80% of datasets. The components are described in section 5.

associated with interactions between other terms (ΔP_{cross}). The first two terms, ΔP_{qadv} and ΔP_{qres}, are the thermodynamic components of rainfall change, and the next two terms, ΔP_{weak} and ΔP_{shift}, are the dynamic components. In the following analysis, we combine ΔP_{qadv} and ΔP_{weak} (qadvw) because of physically understood cancellations between them: namely, enhanced moisture advection from the oceans increases precipitation most in present-day ascent regions, whereas the weakening tropical circulation reduces precipitation most in the same regions (Chadwick et al. 2013, 2016b; Kent et al. 2015).

Figure 6 shows how the components of this decomposition contribute to the CMIP5 spread in total rainfall change for each East African region. Uncertainty in the projections is clearly dominated by uncertainty in the spatial shifts in convection and its covariance with ΔP_{qres} and ΔP_{cross} (the latter is not shown). Kent et al. (2015) draw similar conclusions for East Africa, using a smaller sample of models and a less tailored region, as well as for the tropics as a whole in the solsticial seasons. These spatial shifts in convection are clarified here as changes in "regional dynamics," meaning either changes in dynamics that are geographically restricted to (or close to) East Africa or the local impacts unique to East Africa of changes in remote dynamics or global processes. Section 4 suggests that this uncertainty in regional dynamics is driven by both the uniform component of marine warming (e.g., via uncertainties in land–sea contrast and atmospheric response to this contrast) and the pattern component of marine warming.

In contrast, the net effect of changes in moisture advected from the ocean and of tropical circulation weakening (qadvw) is more consistently modeled and always leads to an increase in East African rainfall. Similarly, the impact of residual moisture changes over land (ΔP_{qres}) is consistently small and usually positive. The robust increase of the former is consistent with an observed increase in tropical mean precipitation (Allan et al. 2010). Otherwise, we suggest here that physical understanding of $\Delta P_{\text{qadv}} + \Delta P_{\text{weak}}$ and ΔP_{qres} is not yet sufficiently mature to judge whether this mechanistic consensus among large-scale climate models of their small role in projection uncertainty has a physically reliable basis or instead may be subject to systematic errors. Last, the cross terms have a mean close to zero for all regions and also contribute little to total uncertainty. This term is judged reliably small because changes in q and M are generally smaller than their climatologies, and this term ($\Delta q \Delta M$) is a multiplication of anomalies not involving climatologies.

So with regards to developing an understanding of the drivers of uncertainty in the rainfall projections, these results indicate that we should focus on regional dynamical mechanisms (defined above), rather than tropically coherent processes such as the "wet get wetter" mechanism or tropics-wide circulation weakening. This route for further analysis applies to both East African wet seasons.

6. Regional versus remote mechanisms

Thus far, we have examined the relative contributions made by a number of top-level mechanisms to the uncertainty in projected East African rainfall change. We now examine the geographic foci of these mechanisms, noting that previous studies (reviewed in section 1) suggest that there is likely to be a mix of mechanisms located remotely from the region of interest and

located much closer to the region of interest. In an RCM projection, a dominance of remote mechanisms transmitted to Africa will be illuminated by a strong dependence on the driving GCM data (i.e., the RCM acts simply as a downscaling tool), whereas a dominance of more local mechanisms will be illuminated by a dependence on the RCM's own formulation, such that it diverges from the GCM. Our study specifically takes advantage of these contrasting influences on RCM projections by applying a novel analysis of the CORDEX-Africa data to determine the extent to which projection uncertainty is driven by a lack of confidence in mechanisms acting beyond Africa versus a lack of confidence in mechanisms within the African region.

Table 2 shows the matrix of available CORDEX-Africa simulations, whereby a variety of RCMs have been forced at their lateral and marine boundaries by a variety of GCMs for both the historical and RCP8.5 scenarios. Figure 2 shows these 11 GCMs are approximately evenly distributed across projected East African rainfall anomalies, including the high outliers. However, a difficulty is that the variance decomposition we will employ for geographic decomposition of projection uncertainty ideally requires that Table 2 is complete, whereas in practice, many entries are missing because it was prohibitive for climate institutes to run all GCM–RCM combinations. Our solution is to statistically emulate East African climate change for these missing experiments. We use a technique that is a special case of that described by Déqué et al. (2007), iteratively deriving a solution by minimizing the interdependence of global and regional sources of uncertainty. Details are provided in appendix B.

With a complete version of Table 2, it is then straightforward to apply an analysis of variance (ANOVA) to compute the two geographic contributions to total projection uncertainty. First, the inter-RCM variance under consistent external forcing σ^2_{Reg} is computed from the average of the variances across each row of Table 2. This is the contribution from uncertain mechanistic processes within the African domain. Second, the impact of the inter-GCM variance of the boundary data applied to a consistent set of RCMs σ^2_{Glo} is computed as the average variance of the columns of Table 2. This is the contribution of uncertain mechanisms beyond the African domain. Note that σ^2_{Reg} and σ^2_{Glo} also include random internal variations, found at regional and global scales, respectively. This creates a scale dependence of the variance decomposition, with a slight tendency for σ^2_{Reg} to decline at larger scales because spatial averaging reduces the impact of small-scale random variability but not that of large-scale, remote, non-African random variability.

To check the viability of this emulation-and-ANOVA methodology, σ^2_{Reg} was instead computed using the average of the inter-RCM variances calculated for the three GCMs that were used to force at least three RCMs, without emulating any of the missing RCM responses. Similarly, an alternative σ^2_{Glo} was computed using the average inter-GCM variance calculated only from the three RCMs forced by at least three GCMs, again without emulating missing GCM–RCM combinations. The disadvantages of this approach are (i) inconsistencies in the selection of RCMs available for each GCM (and vice versa) and (ii) the inconsistency in the larger number of GCMs to compute σ^2_{Glo} versus only three GCMs used to compute σ^2_{Reg} (and similarly, the numbers of RCMs used for each variance). Nevertheless, this independent quasi-ANOVA approach produces similar results (spatial correlations of the variance separation for rainfall are 0.87 and 0.77 for MAM and OND, respectively), providing assurance that the emulation methodology does not introduce unfounded outliers to the ensemble.

Results from our emulation-and-ANOVA methodology are shown in Fig. 7, which displays the percentage contribution of mechanisms within and beyond the African domain to the total projection uncertainty of rainfall changes (this total uncertainty is $\sigma^2_{\Delta} = \sigma^2_{\mathrm{Reg}} + \sigma^2_{\mathrm{Glo}}$). In both seasons, and for this particular suite of GCMs and RCMs, σ^2_{Reg} is larger than σ^2_{Glo} across the majority of continental Africa. Thus, uncertainty in the mechanisms of the response over Africa to remote changes plays a larger role at the grid scale than uncertainty in the remote responses that are teleconnected to Africa or uncertainties in the mechanisms of teleconnection to Africa (noting that these remote uncertainties are nevertheless still important). This large role for local uncertainty may, for example, reflect uncertain modeling in the convective response over Africa and/or in local land–atmosphere feedbacks. In part, it also reflects the presence of small-scale random variations.

However, the East African Long Rains appear to be an exception to this broader picture, with uncertain local mechanisms instead being dominated by uncertainties beyond Africa (Fig. 7, left panel). Figure 8 therefore applies the same analysis to MAM tropospheric data. This suggests that projection uncertainty may be communicated to the East African Long Rains via changes in lower-tropospheric moisture content and/or upper-tropospheric zonal flow, but not via changes in lower-tropospheric flow for which $\sigma^2_{\mathrm{Glo}}/\sigma^2_{\Delta}$ shows little spatial coherence. This is examined further in section 7, where it will be shown that this unusual finding for the East

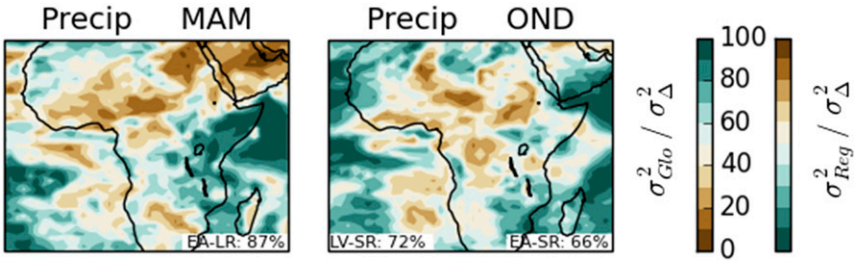

FIG. 7. Percentage of the total projection uncertainty (σ^2_Δ) due to the variance contributions from uncertain mechanistic processes within the CORDEX-Africa domain (σ^2_{Reg}) or uncertain mechanisms beyond the African domain (σ^2_{Glo}). Data are MAM or OND precipitation anomalies. Text inserts are $\sigma^2_{\text{Glo}}/\sigma^2_\Delta$ for data first averaged over the specified region.

African Long Rains encapsulates two distinct types of model behavior. Note that if we remove a potentially common but independent effect of global mean warming on humidity and rainfall across all experiments, this does not affect these conclusions.

During the Short Rains, a more complex and noisy picture is apparent for East African rainfall (Fig. 7, right panel), indicating that this uncertain regional response is due to uncertainties in both local and remote mechanisms.

7. Further analysis of the Long Rains

Sections 3–6 have shown that modeling uncertainties in the change in the Long Rains are mainly due to uncertainties in the regional response to the uniform component of SST warming (more than uncertainties in the warming itself), with a secondary influence from uncertain anomalous SST patterns and a small direct CO_2 impact. These manifest as spatial shifts in convection, driven by uncertain regionally specific dynamical processes rather than globally coherent (thermo)dynamic processes. Additionally, the key regional uncertainties are located beyond Africa, and then communicated to eastern Africa via changes in the lower-tropospheric moisture content and/or upper-tropospheric zonal flow.

The latter of these findings, from the CORDEX data, suggests an obvious route for further analysis, so Fig. 9 examines intermodel correlations between projected MAM East African rainfall anomalies and the tropics-wide lower-tropospheric moisture content or upper-tropospheric zonal flow using data from

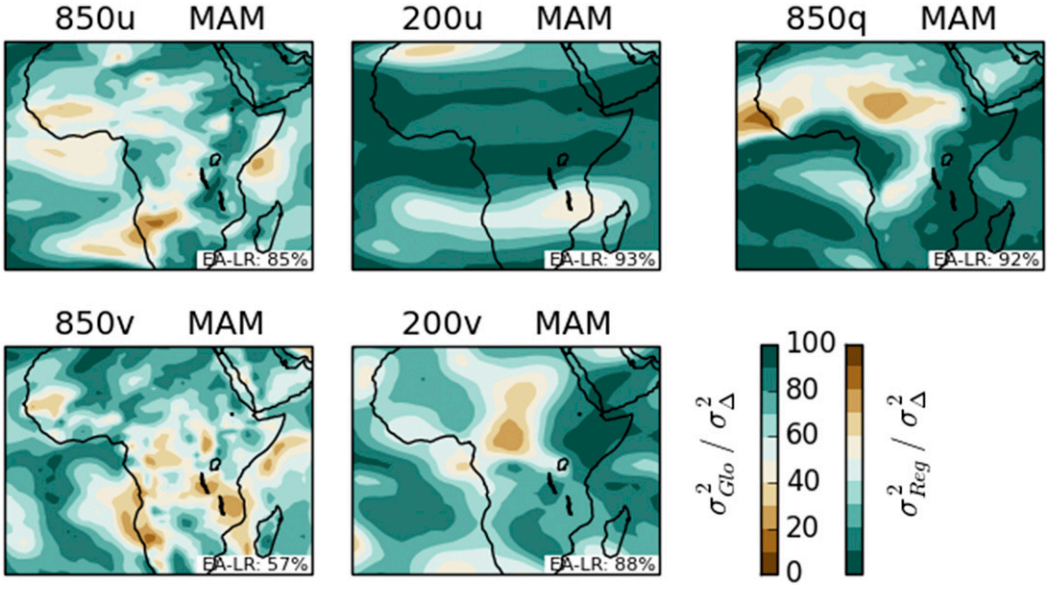

FIG. 8. As in Fig. 7, but data are MAM anomalies for precipitation, 850- and 200-hPa zonal wind (u), 850-hPa specific humidity (q), and 850- and 200-hPa meridional wind (v).

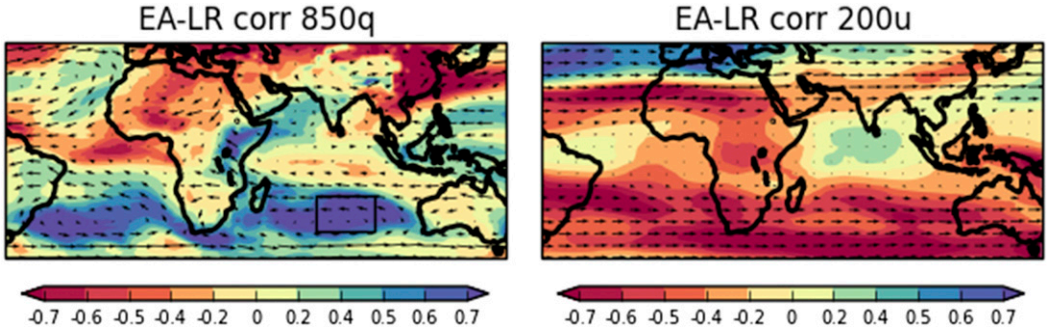

FIG. 9. Maps of the correlation between the change in average EA-LR precipitation and the local change in (left) 850-hPa specific humidity or (right) 200-hPa zonal wind. Correlations are computed across the 11 global coupled models used in CORDEX, using CMIP5 RCP8.5-minus-historical MAM averaged data, scaled by each model's change in global annual mean surface air temperature. Vectors show the ensemble mean climatological 850- or 200-hPa historical flow, and the box in the left panel marks the southern Indian Ocean region analyzed in section 7.

the RCP8.5-minus-historical fully coupled simulations. For consistency with section 6, we use only the 11 coupled models employed by CORDEX. Also, data are scaled by each model's global mean warming to remove this potentially common independent influence on each variable. Correlations with the 200-hPa equatorial flow are weak, suggesting this is unlikely to be the source of the uncertain East African rainfall projections in CORDEX. However, in the lower troposphere, an arc of high correlations connects the southern Indian Ocean with East Africa, following the mean flow and suggesting that advection of uncertain changes in southern Indian Ocean moisture content contribute to uncertainty in the change in Long Rains.

This is further examined by Fig. 10a, which shows the intraensemble relationships between the change in southern Indian Ocean moisture content and the change in the Long Rains. For the coupled models used in CORDEX (black dots), this relationship explains around 60% of the variance in the Long Rains response ($r = 0.78$). However, when all 40 CMIP5 models are considered (gray and black dots), this correlation falls to $r = 0.39$, since the majority of the non-CORDEX models add to the cluster of data randomly distributed in the lower-left quadrant. Thus, the contribution that uncertain changes in moisture content above the Indian Ocean make to uncertain change in the Long Rains is entirely due to two outlying models, which are the two variants of IPSL-CM5A. Without these models, this moisture–rainfall relationship is absent ($r = 0.02$), and EA-LR $\sigma^2_{\mathrm{Glo}}/\sigma^2_{\Delta}$ falls from 87% to 59% (i.e., similar to the Short Rains).

Nevertheless, if the extreme changes projected by IPSL-CM5A can be understood, this may facilitate the

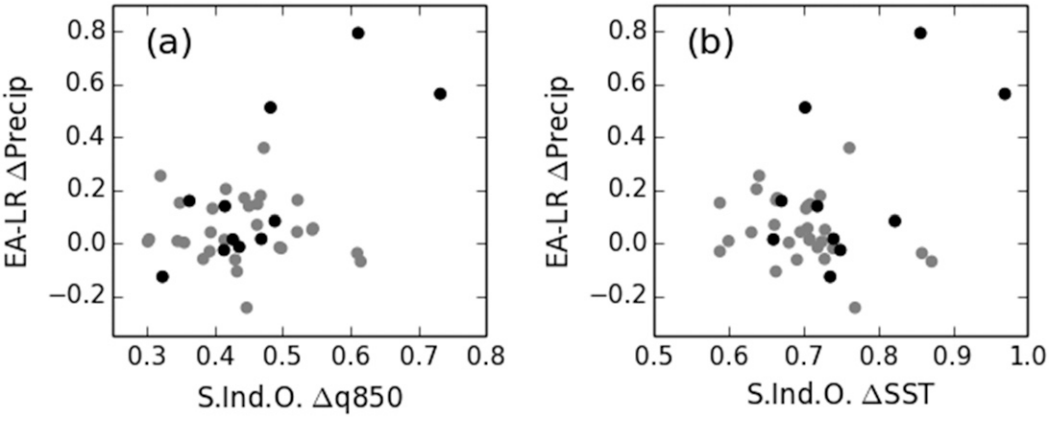

FIG. 10. Scatterplots of the change in (a) 850-hPa specific humidity or (b) SSTs, both averaged over the southern Indian Ocean (x axes), against the change in precipitation averaged over EA-LR (y axes). Black circles show the 11 global coupled models used in CORDEX, and gray circles show the remaining CMIP5 models. Data are RCP8.5-minus-historical MAM averages, scaled by each model's change in global annual mean surface air temperature.

development of a tailored performance metric with the potential to determine whether or not these outlying projections are plausible. Investigating further, Fig. 10b shows the cross-model relationship between projected changes in southern Indian Ocean SSTs and changes in the Long Rains, with $r = 0.57$ for CORDEX GCMs and $r = 0.28$ for all models. This suggests that a component of the IPSL-CM5A models' exceptional increase in the East African Long Rains is due to unusually large SST increases in this region. In fact, these models' exceptional MAM warming occurs throughout the southern subtropical oceans (25°–45°S; not shown), although presumably it is the Indian Ocean manifestation that impacts eastern Africa. This exhibits as a relatively large ΔP_{qres} anomaly over East Africa, where local dynamic feedbacks presumably cause the large ΔP_{shift} anomalies (not shown).

In summary, Figs. 9 and 10 have begun to explain the IPSL-CM5A models' exceptional projection for the Long Rains. Further study is ongoing to more fully understand the causes of these models' outlying behavior and assess its plausibility. Once the trustworthiness of the mechanisms driving IPSL-CM5A's exceptional projections has been established, it will be possible to either downweight them or perhaps remove them as implausible outliers or perhaps continue to retain their projections as a worst-case scenario. All outcomes would be informative for stakeholders.

8. Conclusions

The aim of this study has been to begin to understand the causes of uncertainty among models' projections of tropical regional seasonal rainfall change. Our focus has been on East Africa's two wet seasons, but the synthesis of techniques employed here may also prove useful for understanding projection uncertainty for other tropical terrestrial regions. One motivation for this work, once the understanding of the causes of uncertainty is more fully developed, is to be able to derive projection-relevant metrics of models' current climate performance. It has been common practice to date to discount or downweight models that perform poorly against standard metrics (e.g., the magnitude of spatial and seasonal error patterns), but Rowell et al. (2016) have shown that for East Africa, this is ineffectual for reducing projection spread (with other studies reaching similar conclusions for other regions; e.g., Déqué and Somot 2010; Knutti et al. 2010; Monerie et al. 2017). Thus, more sophisticated metrics are required that discriminate between models in a way that is specifically tailored to their projected regional climate change, providing a more robust basis for narrowing the CMIP uncertainty range.

Section 2 employed point-to-point intermodel correlations to show that the relative deviation of each model's projected anomaly from that of other models varies considerably across the East African region and also between the two wet seasons. This indicates that the causes of projection uncertainty have considerable spatial and seasonal variability, thus motivating a careful derivation of spatial averaging regions within which intermodel projection behavior is relatively homogeneous (and hence, also the driver of projection uncertainty). A moderately large East African region was separately defined for each wet season, as well as a smaller Lake Victoria–based region for the Short Rains.

The bulk of the study then examined the results of four complementary experimental and decomposition techniques to begin to unravel the drivers of East African projection uncertainty. Novel elements were their application to a specific region (rather than a generic tropics-wide application), the simplification and application of an ANOVA technique to the relatively new CORDEX data, and the synthesis of results from all four techniques.

For the Short Rains, it was shown that modeling uncertainty in projected rainfall change is caused by uncertainties in the regional response to both the uniform and pattern components of SST warming (and not uncertainties in the magnitude of warming itself), with direct CO_2 effects playing a secondary role. These manifest as spatial shifts in convection driven by uncertain regional dynamical mechanisms, rather than globally coherent (thermo)dynamic mechanisms. Geographically, these ''regional dynamical mechanisms'' are both the changes in dynamics that are restricted to (or close to) East Africa and the local impacts (unique to East Africa) of changes in remote dynamics or global processes.

For the Long Rains region, most conclusions are similar. However, uncertainties in the response to the uniform component of SST warming appear to be more important than uncertainties in the atmospheric response to a fixed pattern of SST change (at least for the CMIP3 average pattern of change and for models that performed idealized AGCM experiments). A particularly revealing difference was also the apparently large role of uncertainties located beyond Africa. This was found to reflect the behavior of two outlying models, rather than that of the majority. These are the low- and medium-resolution versions of IPSL-CM5A, both of which experience exceptional warming in the southern subtropical oceans. This leads to a large increase in lower-tropospheric moisture content, which is advected by the mean flow from the southern Indian Ocean to

East Africa, contributing to feedbacks on convection and to an exceptional increase in Long Rains totals. If this contrast in behavior between IPSL-CM5A and the majority of models can be related to their present-day performance, then the reliability of these exceptional projections (rainfall increases of 52% and 120%) could be established, providing useful information for communication to decision-makers.

Further work must now determine whether there are other causes of the IPSL-CM5A exceptional Long Rains projections and use this alongside the above outcomes to develop observational constraints for this pair of models versus the majority. Refinement of the projected range for both seasons will then require an understanding of the contrasting projections among the majority of models. This will need to focus on uncertainties in East Africa's local response to the general warming, as well as uncertainties in the teleconnections from remote regions, such as those due to altered SST patterns. A further critical issue, also raised in section 1, is that CMIP models may present a biased ensemble: for example, this could be due to systematic effects from the use of parameterized convection, the lack of coupling with East Africa's Great Lakes, and the absence of growing urban land use. It is essential to investigate the extent of such biases, to determine the most affected climatic parameters, and to estimate the potential further impact on the uncertainties communicated to decision-makers.

Acknowledgments. DPR was funded by the U.K. Department for International Development (DFID)/Natural Environment Research Council (NERC) Future Climate for Africa (FCFA) HyCRISTAL project (NE/M019985/1), and RC was supported by the Newton Fund through the Met Office Climate Science for Service Partnership Brazil (CSSP Brazil). The many modeling groups listed in Tables 1 and 2 are gratefully acknowledged for producing and making their simulations available, as is the World Climate Research Programme Working Group on Coupled Modelling (WCRP-WGCM) for taking responsibility for the CMIP5 and CORDEX model archives, and the U.S. Department of Energy's Program for Climate Model Diagnosis and Intercomparison (PCMDI) for archiving the model output.

APPENDIX A

Determination of the Branch Time of CMIP5 abrupt4xCO$_2$ Experiments

To determine the direct radiative effect of a model's instantaneous quadrupling of CO_2, which evolves over just a few weeks, it is essential to know the exact year in which the abrupt4xCO_2 experiment branches from the piControl. Unfortunately this parameter is not always present in the CMIP5 models' metadata, and it can be ambiguous or unreliable. Here, we present a methodology to determine this date.

Essentially, we take advantage of the knowledge that the ocean surface evolves more slowly than the atmosphere. After the abrupt change in external forcing, it is expected that SSTs in the abrupt4xCO_2 experiment will diverge much less rapidly from the piControl than the atmospheric data. All models branch these experiments at 1 January, except HadGEM2-ES, which branches at 1 December. Therefore, to determine the piControl branch year, we compute the root-mean-square difference (RMSD) of the global SST field between the initial January mean from abrupt4xCO_2 and all January means from piControl (or December means for HadGEM2-ES). The hypothesis is that a distinct minimum of RMSD will be found in the branch year. To facilitate a display of results amalgamated across models, the minimum of each model's RMSDs is removed, and the remaining values are allocated to 20 equal-sized bins spanning the remaining range. Further bins of the same size are then added below this range, into which the minimum RMSD of each model is placed (noting that bin size varies between models). If a model's minimum RMSD were to be indistinct from that of other years, then it would appear in the bin immediately adjacent to the main set of 20 bins.

Results are shown in Fig. A1. It is clear that for all models, the minimum RMSD is distinct from RMSDs with the other piControl years (evidenced by a gap of at least two vacant bins), demonstrating that this approach confidently identifies the branch year of each abrupt4xCO_2 experiment. These years are recorded in Table 1.

APPENDIX B

Emulation of Missing CORDEX Models

Table 2 shows the GCM–RCM combinations run under the CORDEX protocol. The problem for the variance decomposition of section 6 is that many combinations are missing due to resource limitations. Nevertheless, some GCMs were used to force a larger number of RCMs, and some RCMs were forced by a larger number of GCMs. This higher population in some rows and columns provides an opportunity for completion of the matrix. We follow the methodology of Déqué et al. (2007), applying a special case of their approach since we have a two-dimensional matrix rather than their four-dimensional matrix. This iterates toward a solution by minimizing the covariance between GCM and RCM contributions.

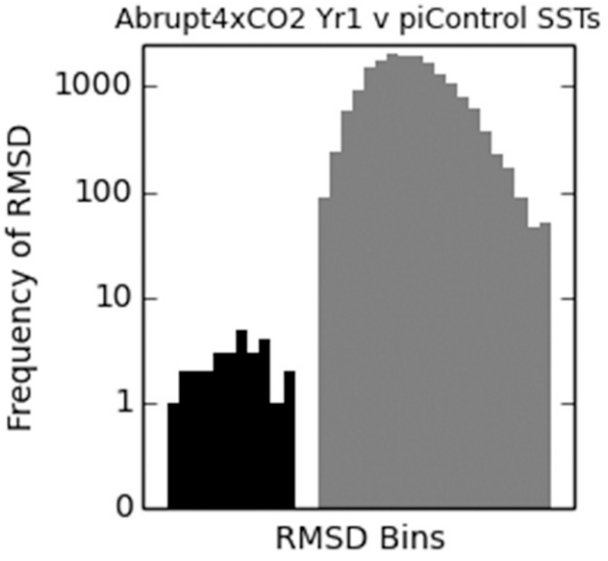

FIG. A1. Histogram of the RMSDs of global SST patterns between the first abrupt4xCO_2 January mean and all piControl January means (December for HadGEM2-ES). Black bars are each model's minimum RMSD, and gray bars are RMSDs for all other piControl years.

In our case, the algorithm reduces to a two-step process. The notation is that X_{rg} represents the RCP8.5-minus-historical climate anomaly of a given variable for RCM r forced by GCM g. The climate anomaly X_{rg} may be a gridpoint datum or a spatial average, computed for the multidecadal means specified in section 2a. The first step is that three types of average over X are computed as follows: over all available RCM projections for each GCM ($\bar{X}_g$), over all available projections for each RCM ($\bar{X}_r$), and over the full set of available GCM–RCM combinations ($\overline{\bar{X}}$). The second step is that data for all missing GCM–RCM combinations are computed as

$$X_{\mathrm{rg}} = \bar{X}_g + \bar{X}_r - \overline{\bar{X}}\,.$$

This pair of calculations is then iterated 50 times, with new values of $\bar{X}_g$, $\bar{X}_r$, and $\overline{\bar{X}}$ computed at each iteration, incorporating the new data for the missing experiments (data for available GCM–RCM experiments are never adjusted). Root-mean-squares across the matrix of the differences among each iteration converge to less than 1% of the matrix mean, using either gridpoint data or spatial averages, demonstrating the successful convergence of the iterative process.

REFERENCES

Allan, R. P., B. J. Soden, V. O. John, W. Ingram, and P. Good, 2010: Current changes in tropical precipitation. *Environ. Res. Lett.*, **5**, 025205, https://doi.org/10.1088/1748-9326/5/2/025205.

Bayr, T., and D. Dommenget, 2013: The tropospheric land–sea warming contrast as the driver of tropical sea level pressure changes. *J. Climate*, **26**, 1387–1402, https://doi.org/10.1175/JCLI-D-11-00731.1.

Berg, A., and Coauthors 2016: Land–atmosphere feedbacks amplify aridity increase over land under global warming. *Nat. Climate Change*, **6**, 869–874, https://doi.org/10.1038/nclimate3029.

Bony, S., G. Bellon, D. Klocke, S. Sherwood, S. Fermepin, and S. Denvil, 2013: Robust direct effect of carbon dioxide on tropical circulation and regional precipitation. *Nat. Geosci.*, **6**, 447–451, https://doi.org/10.1038/ngeo1799.

Byrne, M. P., and P. A. O'Gorman, 2016: Understanding decreases in land relative humidity with global warming: Conceptual model and GCM simulations. *J. Climate*, **29**, 9045–9061, https://doi.org/10.1175/JCLI-D-16-0351.1.

Camberlin, P., and N. Philippon, 2002: The East African March–May rainy season: Associated atmospheric dynamics and predictability over the 1968–97 period. *J. Climate*, **15**, 1002–1019, https://doi.org/10.1175/1520-0442(2002)015<1002:TEAMMR>2.0.CO;2.

Cao, L., G. Bala, and K. Caldeira, 2012: Climate response to changes in atmospheric carbon dioxide and solar irradiance on the time scale of days to weeks. *Environ. Res. Lett.*, **7**, 034015, https://doi.org/10.1088/1748-9326/7/3/034015.

Chadwick, R., I. Boutle, and G. Martin, 2013: Spatial patterns of precipitation change in CMIP5: Why the rich do not get richer in the tropics. *J. Climate*, **26**, 3803–3822, https://doi.org/10.1175/JCLI-D-12-00543.1.

——, P. Good, T. Andrews, and G. Martin, 2014: Surface warming patterns drive tropical rainfall pattern responses to CO_2 forcing on all timescales. *Geophys. Res. Lett.*, **41**, 610–615, https://doi.org/10.1002/2013GL058504.

——, ——, G. Martin, and D. P. Rowell, 2016a: Large rainfall changes consistently projected over substantial areas of tropical land. *Nat. Climate Change*, **6**, 177–181, https://doi.org/10.1038/nclimate2805.

——, ——, and K. Willett, 2016b: A simple moisture advection model of specific humidity change over land in response to SST warming. *J. Climate*, **29**, 7613–7632, https://doi.org/10.1175/JCLI-D-16-0241.1.

——, H. Douville, and C. B. Skinner, 2017: Timeslice experiments for understanding regional climate projections: Applications to the tropical hydrological cycle and European winter circulation. *Climate Dyn.*, **49**, 3011–3029, https://doi.org/10.1007/s00382-016-3488-6.

Chou, C., and J. D. Neelin, 2004: Mechanisms of global warming impacts on regional tropical precipitation. *J. Climate*, **17**, 2688–2701, https://doi.org/10.1175/1520-0442(2004)017<2688:MOGWIO>2.0.CO;2.

——, ——, C.-A. Chen, and J.-Y. Tu, 2009: Evaluating the "rich-get-richer" mechanism in tropical precipitation change under global warming. *J. Climate*, **22**, 1982–2005, https://doi.org/10.1175/2008JCLI2471.1.

Collins, M., and Coauthors, 2013: Long-term climate change: Projections, commitments and irreversibility. *Climate Change 2013: The Physical Science Basis*, T. F. Stocker et al., Eds., Cambridge University Press, 1029–1136.

Déqué, M., and S. Somot, 2010: Weighted frequency distributions express modelling uncertainties in the ENSEMBLES regional climate experiments. *Climate Res.*, **44**, 195–209, https://doi.org/10.3354/cr00866.

——, and Coauthors, 2007: An intercomparison of regional climate simulations for Europe: Assessing uncertainties in model

projections. *Climatic Change*, **81** (Supp. 1), 53–70, https://doi.org/10.1007/s10584-006-9228-x.

Dong, B.-W., J. M. Gregory, and R. T. Sutton, 2009: Understanding land–sea warming contrast in response to increasing greenhouse gases. Part I: Transient adjustment. *J. Climate*, **22**, 3079–3097, https://doi.org/10.1175/2009JCLI2652.1.

Fasullo, J. T., 2010: Robust land–ocean contrasts in energy and water cycle feedbacks. *J. Climate*, **23**, 4677–4693, https://doi.org/10.1175/2010JCLI3451.1.

——, 2012: A mechanism for land–ocean contrasts in global monsoon trends in a warming climate. *Climate Dyn.*, **39**, 1137–1147, https://doi.org/10.1007/s00382-011-1270-3.

Giannini, A., 2010: Mechanisms of climate change in the semiarid African Sahel: The local view. *J. Climate*, **23**, 743–756, https://doi.org/10.1175/2009JCLI3123.1.

Giorgi, F., C. Jones, and G. R. Asrar, 2009: Addressing climate information needs at the regional level: The CORDEX framework. *WMO Bull.*, **58**, 175–183, https://public.wmo.int/en/bulletin/addressing-climate-information-needs-regional-level-cordex-framework.

He, J., and B. J. Soden, 2016: Does the lack of coupling in SST-forced atmosphere-only models limit their usefulness for climate change studies? *J. Climate*, **29**, 4317–4325, https://doi.org/10.1175/JCLI-D-14-00597.1.

Held, I. M., and B. J. Soden, 2006: Robust responses of the hydrological cycle to global warming. *J. Climate*, **19**, 5686–5699, https://doi.org/10.1175/JCLI3990.1.

——, T. L. Delworth, J. Lu, K. L. Findell, and T. R. Knutson, 2005: Simulation of Sahel drought in the 20th and 21st centuries. *Proc. Natl. Acad. Sci. USA*, **102**, 17 891–17 896, https://doi.org/10.1073/pnas.0509057102.

Hillbruner, C., and G. Moloney, 2012: When early warning is not enough—Lessons learned from the 2011 Somalia famine. *Global Food Secur.*, **1**, 20–28, https://doi.org/10.1016/j.gfs.2012.08.001.

Jones, C., F. Giorgi, and G. Asrar, 2011: The Coordinated Regional Downscaling Experiment: CORDEX, an international downscaling link to CMIP5. *CLIVAR Exchanges*, No. 16, International CLIVAR Project Office, Southampton, United Kingdom, 34–40.

Kang, S. M., and I. M. Held, 2012: Tropical precipitation, SSTs and the surface energy budget: A zonally symmetric perspective. *Climate Dyn.*, **38**, 1917–1924, https://doi.org/10.1007/s00382-011-1048-7.

Kent, C., R. Chadwick, and D. P. Rowell, 2015: Understanding uncertainties in future projections of seasonal tropical precipitation. *J. Climate*, **28**, 4390–4413, https://doi.org/10.1175/JCLI-D-14-00613.1.

Knutti, R., R. Furrer, C. Tebaldi, J. Cermak, and G. A. Meehl, 2010: Challenges in combining projections from multiple models. *J. Climate*, **23**, 2739–2758, https://doi.org/10.1175/2009JCLI3361.1.

——, D. Masson, and A. Gettelman, 2013: Climate model genealogy: Generation CMIP5 and how we got there. *Geophys. Res. Lett.*, **40**, 1194–1199, https://doi.org/10.1002/grl.50256.

Long, S.-M., S.-P. Xie, X.-T. Zheng, and Q. Liu, 2014: Fast and slow responses to global warming: Sea surface temperature and precipitation patterns. *J. Climate*, **27**, 285–299, https://doi.org/10.1175/JCLI-D-13-00297.1.

Ma, J., and S.-P. Xie, 2013: Regional patterns of sea surface temperature change: A source of uncertainty in future projections of precipitation and atmospheric circulation. *J. Climate*, **26**, 2482–2501, https://doi.org/10.1175/JCLI-D-12-00283.1.

——, ——, and Y. Kosaka, 2012: Mechanisms for tropical tropospheric circulation change in response to global warming. *J. Climate*, **25**, 2979–2994, https://doi.org/10.1175/JCLI-D-11-00048.1.

Marsham, J., and Coauthors, 2015: First HyCRISTAL workshop—Integrating hydroclimate science into policy decisions for climate-resilient infrastructure and livelihoods in East Africa. *GEWEX News*, No. 4, International GEWEX Project Office, Silver Spring, MD, 23–24.

Mason, J. B., J. M. White, L. Heron, J. Carter, C. Wilkinson, and P. Spiegel, 2012: Child acute malnutrition and mortality in populations affected by displacement in the Horn of Africa, 1997–2009. *Int. J. Environ. Res. Public Health*, **9**, 791–806, https://doi.org/10.3390/ijerph9030791.

Merlis, T., 2015: Direct weakening of tropical circulations from masked CO_2 radiative forcing. *Proc. Natl. Acad. Sci. USA*, **112**, 13 167–13 171, https://doi.org/10.1073/pnas.1508268112.

Monerie, P. A., E. Sanchez-Gomez, and J. Boé, 2017: On the range of future Sahel precipitation projections and the selection of a sub-sample of CMIP5 models for impact studies. *Climate Dyn.*, **48**, 2751–2770, https://doi.org/10.1007/s00382-016-3236-y.

Nicholson, S. E., 2014: A detailed look at the recent drought situation in the Greater Horn of Africa. *J. Arid Environ.*, **103**, 71–79, https://doi.org/10.1016/j.jaridenv.2013.12.003.

——, 2016: An analysis of recent rainfall conditions in eastern Africa. *Int. J. Climatol.*, **36**, 526–532, https://doi.org/10.1002/joc.4358.

——, 2017: Climate and climatic variability of rainfall over eastern Africa. *Rev. Geophys.*, **55**, 590–635, https://doi.org/10.1002/2016RG000544.

Nikulin, G., and Coauthors, 2012: Precipitation climatology in an ensemble of CORDEX-Africa regional climate simulations. *J. Climate*, **25**, 6057–6078, https://doi.org/10.1175/JCLI-D-11-00375.1.

Ogallo, L. J., J. E. Janowiak, and M. S. Halpert, 1988: Teleconnection between seasonal rainfall over East Africa and global sea surface temperature anomalies. *J. Meteor. Soc. Japan*, **66**, 807–822, https://doi.org/10.2151/jmsj1965.66.6_807.

Otieno, V. O., and R. O. Anyah, 2013: CMIP5 simulated climate conditions of the Greater Horn of Africa (GHA). Part II: Projected climate. *Climate Dyn.*, **41**, 2099–2113, https://doi.org/10.1007/s00382-013-1694-z.

Rowell, D. P., 2012: Sources of uncertainty in future changes in local precipitation. *Climate Dyn.*, **39**, 1929–1950, https://doi.org/10.1007/s00382-011-1210-2.

——, 2013: Simulating SST teleconnections to Africa: What is the state of the art? *J. Climate*, **26**, 5397–5418, https://doi.org/10.1175/JCLI-D-12-00761.1.

——, and R. G. Jones, 2006: Causes and uncertainty of future summer drying over Europe. *Climate Dyn.*, **27**, 281–299, https://doi.org/10.1007/s00382-006-0125-9.

——, B. B. B. Booth, S. E. Nicholson, and P. Good, 2015: Reconciling past and future rainfall trends over East Africa. *J. Climate*, **28**, 9768–9788, https://doi.org/10.1175/JCLI-D-15-0140.1.

——, C. A. Senior, M. Vellinga, and R. J. Graham, 2016: Can climate projection uncertainty be constrained over Africa using metrics of contemporary performance? *Climatic Change*, **134**, 621–633, https://doi.org/10.1007/s10584-015-1554-4.

Sanderson, B. M., R. Knutti, and P. Caldwell, 2015: A representative democracy to reduce interdependency in a multimodel

ensemble. *J. Climate*, **28**, 5171–5194, https://doi.org/10.1175/JCLI-D-14-00362.1.

Seto, K. C., B. Güneralp, and L. R. Hutyra, 2012: Global forecasts of urban expansion to 2030 and direct impacts on biodiversity and carbon pools. *Proc. Natl. Acad. Sci. USA*, **109**, 16 083–16 088, https://doi.org/10.1073/pnas.1211658109.

Shongwe, M. E., G. J. van Oldenborgh, B. van den Hurk, and M. van Aalst, 2011: Projected changes in mean and extreme precipitation in Africa under global warming. Part II: East Africa. *J. Climate*, **24**, 3718–3733, https://doi.org/10.1175/2010JCLI2883.1.

Sugi, M., and J. Yoshimura, 2004: A mechanism of tropical precipitation change due to CO_2 increase. *J. Climate*, **17**, 238–243, https://doi.org/10.1175/1520-0442(2004)017<0238:AMOTPC>2.0.CO;2.

Taylor, K. E., R. J. Stouffer, and G. A. Meehl, 2012: An overview of CMIP5 and the experiment design. *Bull. Amer. Meteor. Soc.*, **93**, 485–498, https://doi.org/10.1175/BAMS-D-11-00094.1.

Voigt, A., S. Bony, J.-L. Dufresne, and B. Stevens, 2014: The radiative impact of clouds on the shift of the intertropical convergence zone. *Geophys. Res. Lett.*, **41**, 4308–4315, https://doi.org/10.1002/2014GL060354.

Xie, S.-P., C. Deser, G. A. Vecchi, J. Ma, H. Teng, and A. T. Wittenberg, 2010: Global warming pattern formation: Sea surface temperature and rainfall. *J. Climate*, **23**, 966–986, https://doi.org/10.1175/2009JCLI3329.1.